ACS Photonics

Open Access

pubs.acs.org/journal/apchd5

Article

Probing Nanogap-Dependent Plasmonic Coupling in Gold Nanoparticle Superlattices by Scanning Tunneling Microscopy Induced Light Emission

Yalan Ma,* Bin Lu, Olivier J. F. Martin, and Andreas Stemmer*

Cite This: https://doi.org/10.1021/acsphotonics.4c01408

Read Online

ACCESS | Metrics & More | Article Recommendations | Supporting Information

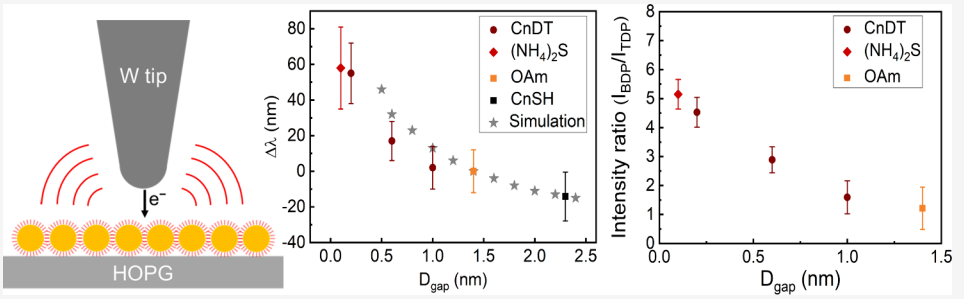

ABSTRACT: Plasmonic nanogaps can support confined and enhanced electromagnetic fields. In this work, we use scanning tunneling microscopy-induced light emission (STM-LE) to study the localized surface plasmon resonance of gold nanoparticle superlattices, which consist of high-density nanogaps of tunable sizes (from 0.1 to 2.3 nm). By analyzing the far-field light emission, we discover that two distinct plasmon modes, i.e., the transverse dipolar plasmon mode (TDP) and bonding dipolar plasmon (BDP) mode, can be selectively excited depending on the location of the STM tip. As the interparticle gap distance decreases, the BDP mode excited at the plasmonic nanogaps shows a monotonous red-shift and broadening, indicating continuously enhanced interparticle plasmonic coupling. Moreover, we observe a stronger radiative strength of the BDP mode compared to the TDP mode excited at the nanoparticles, demonstrating that the plasmonic nanogaps act as electromagnetic hot spots. The intensity ratio of the BDP mode to the TDP mode is enhanced with decreased gap size down to the unprecedent 0.1 nm, revealing the extreme field confinement that can be achieved in plasmonic superlattices. Our results advance the understanding of near-field enhancement in subnanometer plasmonic gaps and shall benefit the design of plasmonic structures for applications in many fields, including surface enhance Raman spectroscopy, photocatalysis, and optoelectronics.

KEYWORDS: *gold nanoparticle superlattice, nanogaps, plasmons, scanning tunneling microscope, light emission, plasmon coupling*

INTRODUCTION

Localized surface plasmons, which are collective oscillations of conduction electrons excited at the metal surface, have attracted significant interest due to their ability to confine and enhance electromagnetic fields.[1,2] A wide variety of metallic nanostructures, such as single nanoparticles (NPs),[3] NP dimers,[4−9] NP on mirror,[10,11] and NP arrays[12] have been developed to facilitate the light-matter interactions in Raman spectroscopy,[13−16] photon sensing,[17] electro-optical devices[18] and nonlinear optical processes.[19,20] Notably, the plasmonic nanogaps (<2 nm) have shown to support a remarkable near-field enhancement, thanks to the capacitive coupling between adjacent plasmons.[4,21] Recently, extended monolayer gold nanoparticle (GNP) superlattices with precisely tunable interparticle gap distance have been presented. Contrary to binary plasmonic systems, such GNP superlattices provide high-density nanogaps and exhibit continuous enhancement of plasmonic coupling when reducing the interparticle gap distance down to 0.1 nm.[12,22] The field enhancement and confinement in the GNP superlattices was evidenced with far-field optical spectroscopy methods.[22] Knowing the details of the near-field information, especially the response of individual nanogaps, is essential for many applications in nano-optics, e.g., single molecule spectroscopy[13] and surface-enhanced Raman spectroscopy.[15]

To understand the local coupling of plasmon resonances, extensive studies have been performed on these nanogaps with both theoretical calculations[7,12,23,24] and experimental measurements. Optical near-field microscopies have provided

Received: July 28, 2024
Revised: December 6, 2024
Accepted: December 6, 2024

opportunities to break the far-field diffraction-limited resolution and explore near-field signatures of individual plasmonic objects.[25] To further improve the spatial resolution, localized excitation by electron microscopy, such as electron energy loss spectroscopy (EELS),[5,26] can be employed to analyze single plasmonic nanostructures. Recently, scanning tunneling microscope (STM) has emerged as a powerful tool for probing the optical properties of metallic nanostructures by measuring the light emission from plasmons excited by inelastic electron tunneling (IET).[27−30] STM electrons can selectively excite plasmons and achieve nanometer-scale resolution.[27,30] For example, using a Au tip, bias-dependent excitation of different plasmon modes was observed in a hexagonal silver nanoparticle monolayer deposited on Au substrate.[31]

In this work, we study the localized plasmonic properties of monolayer GNP superlattices with STM-induced light emission (STM-LE), using nonplasmonic tip and substrate. The nonplasmonic nature of our tip and substrate allows investigation into the more intrinsic plasmonic behavior of nanoparticle superlattices. We also conduct finite elements modeling (FEM)-based numerical simulation to provide a qualitative analysis of the experimental results. In both simulation and experiment, we observe light emission from the radiative decay of different plasmon modes with tip-location-dependent wavelengths and intensities. The plasmon modes excited at the nanogaps are assigned to the bonding dipolar plasmon (BDP) mode, resulting from the hybridization of two horizontal dipolar plasmons of two adjacent GNPs, while the plasmon modes excited at the GNP are assigned to the transverse dipolar plasmon (TDP) mode.[5,7,8,32]

Particularly noteworthy is the higher light emission intensity of the BDP mode compared to the TDP mode, recorded with a sub-NP (<10 nm) spatial resolution. The enhanced intensity of the BDP mode at the nanogaps proves the presence of electromagnetic hot spots at the gaps, due to the strong plasmonic capacitive coupling.[4,12,22] Furthermore, the intensity ratio between the BDP mode and the TDP mode increases with a decreasing gap size, consistent with the simulation result. Additionally, we have observed the wavelength of the BDP mode exhibiting a monotonous red-shift with a decreasing gap size, in good agreement with the trend previously obtained by reflectance measurements on such GNP superlattices.[22] Compared to the far-field measurements, our work provides insights into the near-field plasmonic coupling in individual nanogaps of the GNP superlattices and demonstrates STM-LE as a powerful nanometer-scale probe for studying the optical properties of metallic nanostructures.

RESULTS AND DISCUSSION

Localized surface plasmon properties of GNP superlattices on highly oriented pyrolytic graphite (HOPG) substrate are investigated with STM-LE (see Figure 1a and the Methods section for additional details of the setup). The tunneling electrons serve as a broad-band excitation source with tunable energy and excite localized plasmon modes through the IET process.[29,30] These plasmons can radiatively decay into the far field, generating light emission. Both the intensity and the spectral information on the emitted light are obtained in our experiments. To avoid introducing any tip-induced plasmon, a tungsten tip is utilized due to its nonplasmonic optical properties in the measured wavelength range.[33]

The GNP superlattices with tunable interparticle gap sizes are prepared by interfacial self-assembly combined with

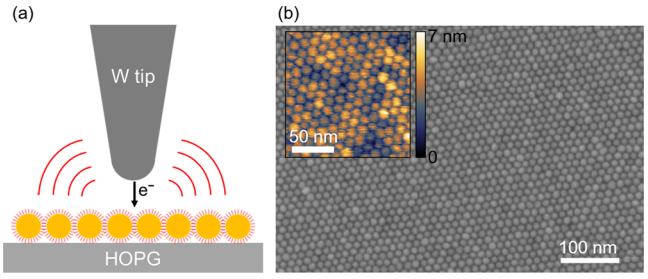

Figure 1. (a) Schematics of the STM-LE experiment. The GNP superlattice (golden spheres) capped with ligands is deposited on the conductive HOPG substrate. Electrons tunneling between the STM tip and the sample excite plasmon modes, which decay radiatively into the far field. (b) Scanning electron microscopy (SEM) image of a GNP superlattice capped with benzene-1,4-dithiol (1,4-BDT) on the HOPG substrate. The inset shows an STM topography image (constant current mode) of the same sample. STM parameters: 100 pA current and −2.5 V tip bias voltage.

subphase exchange and free-floating ligand exchange method (refer to the Methods section for details).[22] The GNPs have a diameter of 13.2 ± 0.5 nm. The interparticle gap size, D_{gap}, is precisely controlled in a range of 0.1−2.3 nm via selection of capping ligands. The as-prepared GNP superlattices are drain-deposited on the HOPG substrate. Figure 1b displays a scanning electron microscope (SEM) image and an STM topography image of a GNP superlattice capped with benzene-1,4-dithiol (1,4-BDT) molecules. The GNP superlattice shows a typical hexagonal close packed pattern. Additional STM topography images of GNP superlattices capped with different molecules are shown in Figure S1 in the Supporting Information. The modification of D_{gap} by altering the capping molecules is apparent in the topography images, as indicated by the count of GNPs per unit length. Meanwhile, the capping molecules introduce an energy barrier in the tunneling process, thus a higher tunneling bias voltage, V, is required to image the GNPs capped with longer molecules, e.g., 1-hexadecanethiol (C16SH). To confirm this, the C16SH-capped GNP superlattice is treated with oxygen plasma to remove the capping molecules. After plasma treatment, cracks appear in the GNP superlattice, indicating the removal of capping molecules and the diminished steric stabilization of GNPs.[34] Consequently, a reduced bias voltage is needed to obtain an STM topography image at the same tunneling current (I), which agrees with a decreased tunneling barrier. Throughout our experiments, all STM-LE measurements are performed on GNP superlattices with capping ligands, where ligands ensure sufficient chemical and steric stabilization for the GNP superlattices.[34]

STM-LE has been reported to probe the radiative electromagnetic local density of states, where the light emission intensity is directly correlated to the local plasmon strength.[28−30] We now study the spatial distribution of the light emission intensity of the GNP superlattices. Figure 2a shows an STM image of a GNP superlattice capped by 1,4-BDT, obtained with a constant tunneling current and tip bias voltage (I = 100 pA, V = −2.5 V). An area of 24 × 24 nm^2 (outlined by the white box in Figure 2a), which contains a complete lattice cell, is evaluated using STM-LE. The surface height distribution with a pixel size of 2 × 2 nm^2 is presented in Figure 2b, while Figure 2c displays the corresponding photon count map acquired with the photon counter (I = 2 nA, V = −3 V). We observe that the photon count is higher at the interparticle gaps compared to the regions on the GNPs.

https://doi.org/10.1021/acsphotonics.4c01408
ACS Photonics XXXX, XXX, XXX−XXX

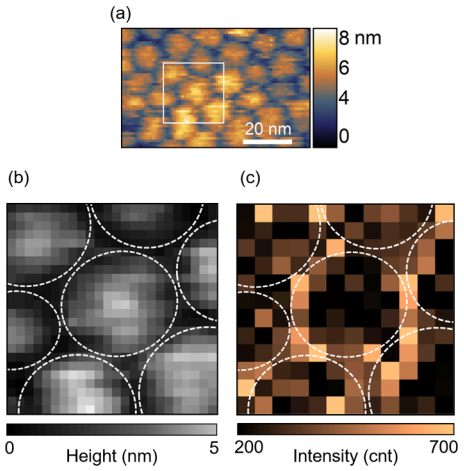

Figure 2. Spatial distribution of the STM-LE intensity. (a) STM image of a GNP superlattice capped with 1,4-BDT on the HOPG substrate. STM parameters: 100 pA current and −2.5 V bias voltage. (b) Height map and (c) corresponding STM-LE intensity acquired in the region (24 × 24 nm^2) indicated by the white box in panel (a). The gaps are marked with dashed lines for better illustration. The pixel size is 2 × 2 nm^2. STM-LE parameters: 2 nA current, −3.0 V bias voltage, and 10 s integration time.

This photon image illustrates that the STM tip indeed excites plasmons that radiatively decay into the far field, and the strength of the plasmon modes depends on the location of the STM tip. Here, we achieve a spatial resolution on a subnanoparticle (<10 nm) scale.

To further investigate the light emission characteristics, we acquire the spectral information at selected tip locations using a spectrometer. Figure 3 shows the experimental results of the light emission as the tip is moved from the center of a nanoparticle (purple dot in Figure 3a) toward the neighboring nanoparticle, crossing the gap (red dot in Figure 3a) and stopped at a position (brown dot in Figure 3a) 8 nm away from the starting position. The step size for this displacement is 1 nm. Figure 3b plots the STM-LE spectra acquired along this trajectory, and Figure 3c compares these normalized STM-LE spectra. When the tip is positioned at the center of the nanoparticle, a resonance peak (λ) appears at a wavelength of ∼755 nm (purple curve, 0 nm). As the tip is moved to the gap, the peak then undergoes a wavelength shift to ∼726 nm (red curve, 6 nm). The spectral intensity at the gap reaches a maximum, consistent with the results obtained by the photon counter (Figure 2c). These results suggest that different plasmon modes are excited on the nanoparticle and at the interparticle gap.

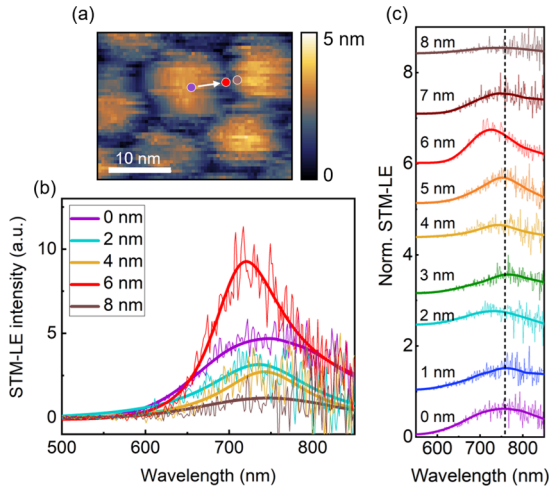

Figure 3. Spatial distribution of the STM-LE intensity. (a) STM image of a GNP superlattice capped with 1,4-BDT on the HOPG substrate. STM parameters: 100 pA current and −2.5 V bias voltage. The tip is moved from the GNP center (purple dot) toward the interparticle gap (red dot), ending at the brown dot, with a 1 nm step size. (b) STM-LE spectra and (c) normalized spectra obtained at locations marked in panel (a). The purple dot in panel (a) is set as the origin (0 nm), and the red dot corresponds to 6 nm. STM-LE parameters: 10 nA current, −3.0 V bias voltage, and 60 s integration time. The spectra in panel (c) are vertically shifted for legibility.

To elucidate the origin of the light emission, we conduct numerical simulations to investigate the plasmon modes excited by tunneling electrons (see the Methods section for further details and Figure S2 in the Supporting Information for additional results). When the excitation is positioned at the center of the GNP, a transverse dipolar plasmon (TDP) mode, oscillating perpendicularly to the superlattice, is generated within this nanoparticle. When the excitation is located at the gap between two GNPs, the surface charge density distribution matches the characteristics of the bonding dipolar plasmon (BDP) mode between the two neighboring GNPs closest to the excitation position.[7,8,32] The calculated radiative strength of the BDP mode is larger than that of the TDP mode, which agrees with the experimental observations (Figure 3). When the excitation is positioned between the particle center and the interparticle gap, both TDP and BDP modes are excited, and the plasmon strength of each mode varies as a function of the excitation position. However, in experimental spectra (1−5 nm in Figure 3), the TDP mode and BDP mode could not be identified, due to the weak signal-to-noise ratio in light emission measurements.

Compared with simulations, the experimental STM-LE exhibits red-shifts and broadening of the TDP and BDP modes. This discrepancy may be attributed to the differences in the dielectric environment, such as the absence of ligands and STM tip in simulations.[35,36] Another explanation could be the deviation in the dielectric constants of GNP and HOPG between simulations and experimental conditions.[37,38] In addition, we simulate the light emission of configurations involving 2 GNPs and 7 GNPs on HOPG substrates (refer to Figures S5 and S6 in the Supporting Information). We observe that the number of GNPs in simulation affects the plasmon wavelength.

Furthermore, contrary to the simulations, the experimental wavelength of the BDP mode is blue-shifted compared to the TDP mode. Analogous to molecular orbital theory, the BDP mode arises from the in-phase coupling between two dipolar plasmons of two nanoparticles and exhibits a red-shift in wavelength compared to the surface plasmon resonance (SPR) of individual nanoparticles.[31,39,40] In our study, the GNPs are deposited on HOPG, wherein the conductive HOPG substrate acts as a mirror and enables a redistribution of the surface charges, resulting in a modification of the plasmon wavelength.[7,32] Moreover, with the additional influence of the experimental environment (STM tip and capping ligands), it is conceivable that the measured wavelength of the BDP is shorter than that of the TDP mode. Similar phenomena will be encountered in GNP superlattices capped with other molecules in subsequent investigations.

https://doi.org/10.1021/acsphotonics.4c01408
ACS Photonics XXXX, XXX, XXX−XXX

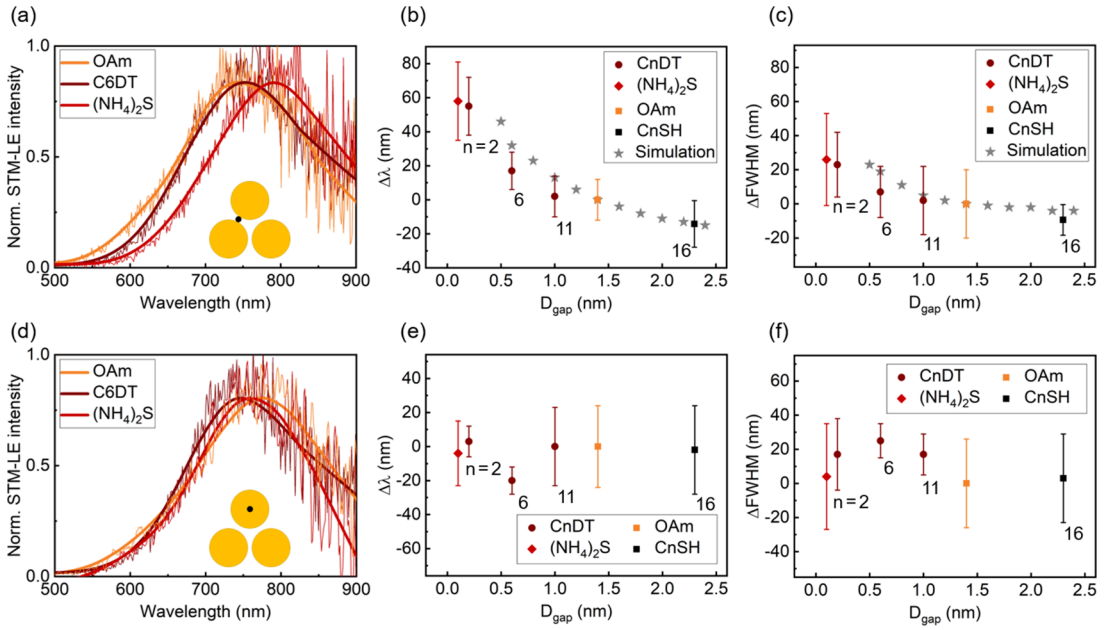

Figure 4. Influence of the interparticle gap size. (a) Normalized STM-LE spectra from GNP superlattices capped with oleylamine (OAm), 1,6-hexanedithiol (C6DT), and ammonium sulfide ($(NH_4)_2S$), excited at the interparticle gaps. (b) Experimental and simulated plasmonic peak wavelength shift, $\Delta\lambda$, and (c) full width at half-maximum (fwhm) shift, Δfwhm, of GNP superlattices capped with different ligands, excited at the interparticle gaps. (d) Normalized STM-LE spectra from GNP superlattices capped with OAm, C6DT, and $(NH_4)_2S$, excited on the center of the GNPs. STM parameters: 5 nA current and −3.0 V bias voltage. (e) Experimental $\Delta\lambda$ and (f) Δfwhm of GNP superlattices capped with different ligands, excited on the center of the GNPs. In panels (a, d), the thin curves are the raw data, and the thick lines correspond to the smoothed results. STM parameters: 5 nA current, −5.0 V bias voltage for C16SH, while 5 nA current and −3.0 V bias voltage for all other molecules. *n* in panels (b, c, e, f) indicates the number of carbon atoms.

The intensity of emitted photons from plasmons generated by IET depends on the bias voltage.[30,41,42] Figure S3 in the Supporting Information shows the bias-dependent STM-LE spectra measured from GNP superlattices capped with short ligands (1,4-BDT) and long ligands (C16SH). Similar to the calculated results, the experimental peak wavelengths of the TDP and BDP modes first blue-shift with increasing bias voltage, and then remain constant when the bias voltage surpasses a threshold value. Moreover, the maximal energy (eV_{bias}) of tunneling electrons exceeds the emitted photon energy, and the onset bias voltage required for detectable light emission increases with longer capping molecules. This observation further points to the tunneling barrier introduced by the ligands. In this work, we always apply a bias voltage above the threshold value to eliminate the influence of the bias voltage when analyzing the plasmon peak wavelengths.

Having demonstrated the ability to selectively excite plasmon modes at different tip locations, we now investigate the gap-size-dependent behavior of the BDP mode and TDP mode. Figure 4a compares the STM-LE spectra by exciting the BDP mode on GNP superlattices capped with different molecules. Each spectrum is the average of spectra acquired from more than 15 interparticle gaps. A wavelength shift of the BDP mode is observed when changing the ligands. Specifically, the BDP mode of GNP superlattice capped with sulfide ($(NH_4)_2S$, D_{gap} = 0.1 nm) exhibits a significant red-shift compared to the sample capped with long oleylamine (OAm, D_{gap} = 1.4 nm). Figure 4b,c summarize the extracted peak wavelength, λ, and the full width at half-maximum (fwhm) of the BDP mode for different samples. The wavelength shift, $\Delta\lambda$, and the fwhm broadening, Δfwhm, are extracted by setting the OAm-capped superlattice as the reference (λ = 734 nm, fwhm = 184 nm). Both the calculated and measured BDP modes experience monotonous red-shifts and broadening with reducing D_{gap}. In the experiment, a 71 nm red-shift of λ and a 35 nm broadening of fwhm are observed when D_{gap} decreases from 2.3 to 0.1 nm. When short ligands are used, the plasmonic coupling between neighboring GNPs is enhanced, leading to a red-shift and broadening of the BDP mode.[7,8] These trends of λ red-shift and fwhm broadening in our results are in good agreement with the results of large-scale optical reflectance measurements obtained from GNPs superlattice on the surface of acetonitrile, with discrepancies of $\Delta\lambda$ and Δfwhm being assigned to the different dielectric environment.[22] The charge-transfer plasmon mode emerging from quantum tunneling between nanoparticles is not observed in our work.[5,12,39] Thus, our results confirm the previous theoretical and experimental observations[12,22] that the plasmonic near-field coupling in extended GNP superlattices with diminishing gap distance differs from the isolated binary systems.[5,10,39] Yet, we notice in Figure 4b that the wavelength shift seems to saturate as we reach very short spacing distances.[43]

Figure 4d–f show the experimental results of the STM-LE spectra obtained by placing the tip on the center of the GNP, where the TDP mode is excited. Again, each spectrum is the average of spectra acquired from the centers of more than 15 GNPs. $\Delta\lambda$ in (e) and Δfwhm in (f), are extracted by setting the OAm-capped superlattice as the reference (λ = 771 nm, fwhm = 200 nm). In contrast to the BDP mode, no significant wavelength shift of the TDP mode is observed in both measurements and calculations (see Figure S4 in the Supporting Information), indicating that the interparticle gap size has negligible influence on the TDP mode. The plasmon

https://doi.org/10.1021/acsphotonics.4c01408
ACS Photonics XXXX, XXX, XXX−XXX

coupling between the excited nanoparticle and the neighboring nanoparticles is normal to the TDP. Similar to nanoparticle dimers, the TDP mode is not sensitive to changes in the gap distance, resulting in a negligible influence on the energy of the TDP mode.[8]

Previously, we have observed enhanced strength of BDP modes for reduced gap sizes. In the following, we investigate the gap-size-dependent light emission intensity. First, we perform line scans on GNP superlattices and acquire the light intensity using the photon counter. Figure 5a and Figure 5b

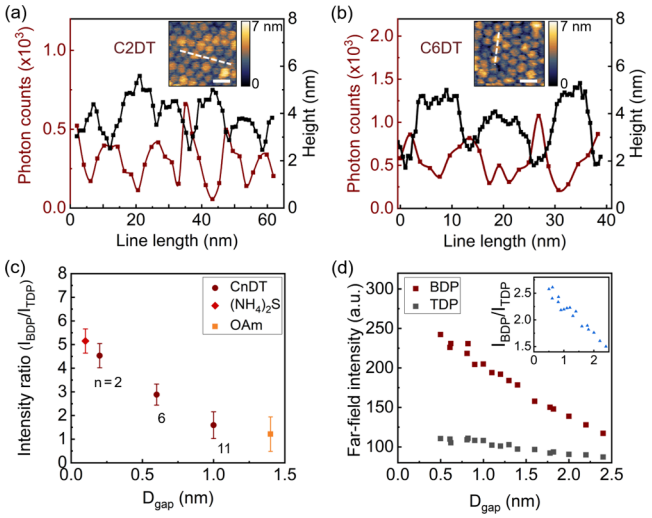

Figure 5. Gap-size-dependent STM-LE intensity. Photon intensity (red curves) and topography height (black curves) from GNP superlattices capped with (a) C2DT and (b) C6DT. Insets show the STM images with the scanned lines marked as dashed lines. Scale bars: 20 nm. (c) Experimental intensity ratio, I_{BDP}/I_{TDP}, of GNP superlattices with different capping ligands. STM-LE parameters: 2 nA current, −3.0 V bias voltage, and 10 s integration time. (d) Calculated intensities of TDP and BDP modes for different gap distances. The inset displays the calculated I_{BDP}/I_{TDP}.

compare the light intensity with the topographic height of two GNP superlattices capped with 1,2-ethanedithiol (C2DT) and 1,6-hexanedithiol (C6DT), respectively. For both samples, the emitted light shows maximal photon numbers at the interparticle gaps (BDP mode) and fewer photons on the particle (TDP mode), as in Figure 2. Meanwhile, the intensity ratio between the BDP mode and TDP mode differs between these two samples. For statistical analysis, we measure the photon counts from more than 30 GNPs and 30 interparticle gaps over an area of 5 μm^2 on different samples. In Figure 5c, the intensity ratio, I_{BDP}/I_{TDP}, is plotted as a function of D_{gap}. In agreement with the simulation result (inset in Figure 5d), I_{BDP}/I_{TDP} increases with decreasing D_{gap}, reaching an experimental value of 5.2 ± 0.5 at D_{gap} = ∼ 0.1 nm.

As displayed in Figure 5d, the calculated intensities for both BDP and TDP modes increase for decreasing D_{gap}, but with different rates. For the TDP mode, with the shortening of ligands, the GNP approaches closer to the HOPG surface, leading to enhanced coupling between the GNP and the substrate and thus a slight intensity enhancement.[10,11] For the BDP mode excited at the gap, the coupling between the plasmon dipoles of the two neighboring GNPs is enhanced when shorter ligands are used, giving rise to an increased intensity. In our extended GNP superlattices, the enhanced plasmonic coupling of the BDP mode is more significant compared to the TDP mode. Thus, the ratio I_{BDP}/I_{TDP} shows a continuous increasing trend with reducing D_{gap}. Again, similar to the monotonous red-shift of BPD mode, the continuous increase of I_{gap}/I_{np} also indicates that no charge transfer plasmon mode is observed in our samples.[22,44] In our work, the observation of hot spots at the plasmonic nanogaps and their gap-size dependent strengths provides valuable insight into the local electromagnetic field in the nanogaps of GNP superlattices.

CONCLUSIONS

Our study provides a comprehensive investigation of the localized surface plasmon resonances of GNP superlattices using STM-LE. By analyzing the emitted light spectra and intensities, we have gained valuable insights into the local plasmonic behavior within individual nanogaps of the superlattice. We have demonstrated the selective excitation of plasmon modes (i.e., TDP mode and BDP mode), achieving a subnanoparticle (<10 nm) spatial resolution. Through a combination of experimental measurements and simulations, we have elucidated the gap-size-dependent behaviors of these different plasmon modes. Particularly, we have observed monotonous red-shifts and broadening of the BDP mode as the interparticle gap distance decreased, which can be attributed to the enhanced plasmonic coupling between adjacent GNPs. This observation is in good agreement with results from large-scale optical reflectance measurements, while STM-LE allows us to provide important details on the optical near-field in plasmonic superlattices. Furthermore, our investigation revealed a significant enhancement in the intensity ratio of the BDP mode to the TDP mode as gap size decreased down to 0.1 nm, demonstrating the extreme field confinement achievable in plasmonic superlattices. Our findings of hot spots at the nanogaps highlight the importance of precise gap-size control in modulating the plasmonic properties of GNP superlattices. In summary, our work lays a solid foundation for further exploration and manipulations of plasmonic phenomena in nanomaterials for a broad range of optical applications, especially those depending on plasmonic nanogaps for strong local field enhancement and confinement, such as surface-enhanced spectroscopy, optical sensing, and optoelectronics.

METHODS

Sample Preparation. The GNP superlattices were fabricated and characterized using methods reported previously.[22] All GNPs used in our experiments have a diameter of 13.2 ± 0.5 nm. The GNP superlattices capped with ligands were deposited onto the freshly cleaved HOPG substrates (SPI Supplies, grade 1). For the C16SH-capped sample, we used oxygen plasma (PVA TePla, GIGAbatch) to remove ligands around the GNPs with a power of 200 W for 10 s.

Simulations. The numerical calculations are performed with finite element modeling (COMSOL Multiphysics 5.6) in the frequency domain. The GNP sample is placed on the HOPG substrate, surrounded by vacuum. A unitary harmonic point dipole placed 1 nm above the sample surface is used as the excitation source.[30] The orientation of the dipole is always normal to the nearest GNP surface, aligned with the tunneling direction.

https://doi.org/10.1021/acsphotonics.4c01408
ACS Photonics XXXX, XXX, XXX−XXX

The whole system is modeled as a sphere with a diameter of 600 nm, surrounded by a perfectly matched layer (thickness: 100 nm). The bottom half sphere represents the HOPG substrate and the remaining part is vacuum. A finite number of GNPs (37 in this simulation), each with a fixed diameter of 13 nm, are arranged in a hexagonal pattern. The interparticle gap size, D_{gap}, is varied in a range of 0.5−2.4 nm. The GNPs are placed on the HOPG surface at a distance of D_{gap}. The refractive index of gold follows the work of Johnson et al.[37] The refractive index of HOPG is adopted from Querry et al.[38] The wavelength-dependent light emission intensity is calculated by integrating the far-field Poynting vector over the half sphere above the sample. The maximal discretization mesh size for the GNPs is set to 2 nm, with a developer-defined adaptive element size used for meshing the rest of the system. Unlike Au tip which can introduce the tip−sample gap plasmon mode, W tip does not introduce additional plasmon modes in the GNP superlattice (see Figure S5 in the Supporting Information). The W tip is treated as a dielectric environment.

STM-LE Setup. All measurements are conducted with a custom-built STM instrument (10^{-7} mbar, room temperature).[45] A lens (Thorlabs, A110-B, NA 0.4) placed at an incident angle of 60° from the sample normal is used to collect the emitted light. The number of photons is acquired by a TE-cooled single-pixel photon counter (Hamamatsu, C13001-01), and the spectral information is detected by a spectrometer (Princeton Instrument, SP2156i, 150 lines/mm grating, Andor, Newton 970P EMCCD). The wavelength range is 400−900 nm for the photon counter and the spectrometer. All experimental spectra are corrected by the normalized detection efficiency (maximum set to 1). Tungsten tips are fabricated by electrochemical etching in NaOH solution and used to avoid any tip-induced plasmonic effect in the measured wavelength range.[45] To minimize the influence of drift, experiments began only after maintaining the target vacuum for at least 24 h.

■ ASSOCIATED CONTENT

Supporting Information

The Supporting Information is available free of charge at https://pubs.acs.org/doi/10.1021/acsphotonics.4c01408.

STM topography images of GNP superlattices capped with different ligands; numerical calculation result: surface charge density distribution, electrical field, far-field light emission spectra, and intensity ratio I_{gap}/I_{np}; bias-voltage-dependent STM-LE spectra (PDF)

■ AUTHOR INFORMATION

Corresponding Authors

Yalan Ma − *Nanotechnology Group, ETH Zürich, Rüschlikon CH-8803, Switzerland;* orcid.org/0000-0002-4772-7042; Email: mayala@ethz.ch

Andreas Stemmer − *Nanotechnology Group, ETH Zürich, Rüschlikon CH-8803, Switzerland*; Email: astemmer@ethz.ch

Authors

Bin Lu − *Nanotechnology Group, ETH Zürich, Rüschlikon CH-8803, Switzerland;* orcid.org/0009-0008-9329-9270

Olivier J. F. Martin − *Nanophotonics and Metrology Laboratory, Swiss Federal Institute of Technology Lausanne (EPFL), Lausanne CH-1015, Switzerland;* orcid.org/0000-0002-9574-3119

Complete contact information is available at: https://pubs.acs.org/10.1021/acsphotonics.4c01408

Notes

The authors declare no competing financial interest.

■ ACKNOWLEDGMENTS

The authors thank Christian Ritz for supporting the simulation, Blerim Veselaj for technical support and the Cleanroom Operations Team of the Binnig and Rohrer Nanotechnology Center (BRNC) for their valuable help and support.

■ REFERENCES

(1) Amendola, V.; Pilot, R.; Frasconi, M.; Maragò, O. M.; Iatì, M. A. Surface plasmon resonance in gold nanoparticles: a review. *J. Phys.: Condens. Matter* **2017**, *29*, No. 203002.

(2) Maier, S. A. *Plasmonics: Fundamentals and Applications*. Vol. *1*. Springer: New York, 2007.

(3) Anker, J. N.; Hall, W. P.; Lyandres, O.; Shah, N. C.; Zhao, J.; Van Duyne, R. P. Biosensing with plasmonic nanosensors. *Nat. Mater.* **2008**, *7*, 442−453.

(4) Barbry, M.; Koval, P.; Marchesin, F.; Esteban, R.; Borisov, A. G.; Aizpurua, J.; Sánchez-Portal, D. Atomistic near-field nanoplasmonics: reaching atomic-scale resolution in nanooptics. *Nano Lett.* **2015**, *15*, 3410−3419.

(5) Scholl, J. A.; García-Etxarri, A.; Koh, A. L.; Dionne, J. A. Observation of quantum tunneling between two plasmonic nanoparticles. *Nano Lett.* **2013**, *13*, 564−569.

(6) Grillet, N.; Manchon, D.; Bertorelle, F.; Bonnet, C.; Broyer, M.; Cottancin, E.; Lermé, J.; Hillenkamp, M.; Pellarin, M. Plasmon coupling in silver nanocube dimers: resonance splitting induced by edge rounding. *ACS Nano* **2011**, *5*, 9450−9462.

(7) Huang, Y.; Ma, L.; Hou, M.; Li, J.; Xie, Z.; Zhang, Z. Hybridized plasmon modes and near-field enhancement of metallic nanoparticle-dimer on a mirror. *Sci. Rep.* **2016**, *6*, 30011.

(8) Wang, H. Plasmonic refractive index sensing using strongly coupled metal nanoantennas: nonlocal limitations. *Sci. Rep.* **2018**, *8*, 9589.

(9) Atay, T.; Song, J. H.; Nurmikko, A. V. Strongly interacting plasmon nanoparticle pairs: from dipole− dipole interaction to conductively coupled regime. *Nano Lett.* **2004**, *4*, 1627−1631.

(10) Hajisalem, G.; Nezami, M. S.; Gordon, R. Probing the quantum tunneling limit of plasmonic enhancement by third harmonic generation. *Nano Lett.* **2014**, *14*, 6651−6654.

(11) Benz, F.; Tserkezis, C.; Herrmann, L. O.; De Nijs, B.; Sanders, A.; Sigle, D. O.; Pukenas, L.; Evans, S. D.; Aizpurua, J.; Baumberg, J. J. Nanooptics of molecular-shunted plasmonic nanojunctions. *Nano Lett.* **2015**, *15*, 669−674.

(12) Takeuchi, T.; Noda, M.; Yabana, K. Operation of quantum plasmonic metasurfaces using electron transport through subnanometer gaps. *ACS Photonics* **2019**, *6*, 2517−2522.

(13) Nie, S.; Emory, S. R. Probing single molecules and single nanoparticles by surface-enhanced Raman scattering. *Science* **1997**, *275*, 1102−1106.

(14) Zhan, C.; Chen, X. J.; Yi, J.; Li, J. F.; Wu, D. Y.; Tian, Z. Q. From plasmon-enhanced molecular spectroscopy to plasmon-mediated chemical reactions. *Nature Reviews Chemistry* **2018**, *2*, 216−230.

(15) Xomalis, A.; Zheng, X.; Demetriadou, A.; Martínez, A.; Chikkaraddy, R.; Baumberg, J. J. Interfering plasmons in coupled nanoresonators to boost light localization and SERS. *Nano Lett.* **2021**, *21*, 2512−2518.

(16) Zhu, W.; Crozier, K. B. Quantum mechanical limit to plasmonic enhancement as observed by surface-enhanced Raman scattering. *Nat. Commun.* **2014**, *5*, 5228.

(17) Fang, Z.; Liu, Z.; Wang, Y.; Ajayan, P. M.; Nordlander, P.; Halas, N. J. Graphene-antenna sandwich photodetector. *Nano Lett.* **2012**, *12*, 3808−3813.
(18) Atwater, H. A.; Polman, A. Plasmonics for improved photovoltaic devices. *Nat. Mater.* **2010**, *9*, 205−213.
(19) Kauranen, M.; Zayats, A. V. Nonlinear plasmonics. *Nat. Photonics* **2012**, *6*, 737−748.
(20) Danckwerts, M.; Novotny, L. Optical frequency mixing at coupled gold nanoparticles. *Phys. Rev. Lett.* **2007**, *98*, No. 026104.
(21) Yang, Y.; Gu, C.; Li, J. Sub-5 nm metal nanogaps: physical properties, fabrication methods, and device applications. *Small* **2019**, *15*, No. 1804177.
(22) Lu, B.; Vegso, K.; Micky, S.; Ritz, C.; Bodik, M.; Fedoryshyn, Y. M.; Siffalovic, P.; Stemmer, A. Tunable Subnanometer Gaps in Self-Assembled Monolayer Gold Nanoparticle Superlattices Enabling Strong Plasmonic Field Confinement. *ACS Nano* **2023**, *17*, 12774−12787.
(23) Bohren, C. F.; Huffman, D. R. *Absorption and scattering of light by small particles*. John Wiley & Sons 2008.
(24) Purcell, E. M.; Pennypacker, C. R. Scattering and absorption of light by nonspherical dielectric grains. *Astrophys. J.* **1973**, *186*, 705−714.
(25) Krenn, J. R.; Dereux, A.; Weeber, J. C.; Bourillot, E.; Lacroute, Y.; Goudonnet, J. P.; Schider, G.; Gotschy, W.; Leitner, A.; Aussenegg, F. R.; Girard, C. Squeezing the optical near-field zone by plasmon coupling of metallic nanoparticles. *Phys. Rev. Lett.* **1999**, *82*, 2590.
(26) Nelayah, J.; Kociak, M.; Stéphan, O.; García de Abajo, F. J.; Tencé, M.; Henrard, L.; Taverna, D.; Pastoriza-Santos, I.; Liz-Marzán, L. M.; Colliex, C. Mapping surface plasmons on a single metallic nanoparticle. *Nat. Phys.* **2007**, *3*, 348−353.
(27) Myrach, P.; Nilius, N.; Freund, H. J. Photon mapping of individual Ag particles on MgO/Mo (001). *Phys. Rev. B* **2011**, *83*, No. 035416.
(28) Martín-Jiménez, A.; Fernández-Domínguez, A. I.; Lauwaet, K.; Granados, D.; Miranda, R.; García-Vidal, F. J.; Otero, R. Unveiling the radiative local density of optical states of a plasmonic nanocavity by STM. *Nat. Commun.* **2020**, *11*, 1021.
(29) Cao, S.; Zapata-Herrera, M.; Campos, A.; Le Moal, E.; Marguet, S.; Dujardin, G.; Kociak, M.; Aizpurua, J.; Borisov, A. G.; Boer-Duchemin, E. Probing the radiative electromagnetic local density of states in nanostructures with a scanning tunneling microscope. *ACS Photonics* **2020**, *7*, 1280−1289.
(30) Ma, Y.; Martin, O. J.; Stemmer, A. Selectively Exciting and Probing Radiative Plasmon Modes on Short Gold Nanorods by Scanning Tunneling Microscope-Induced Light Emission. *ACS Photonics* **2023**, *10*, 743−750.
(31) Silly, F.; Gusev, A. O.; Taleb, A.; Charra, F.; Pileni, M. P. Coupled plasmon modes in an ordered hexagonal monolayer of metal nanoparticles: a direct observation. *Phys. Rev. Lett.* **2000**, *84*, 5840.
(32) Wang, Y.; Li, Z.; Zhao, K.; Sobhani, A.; Zhu, X.; Fang, Z.; Halas, N. J. Substrate-mediated charge transfer plasmons in simple and complex nanoparticle clusters. *Nanoscale* **2013**, *5*, 9897−9901.
(33) Rakić, A. D.; Djurišíc, A. B.; Elazar, J. M.; Majewski, M. L. Optical properties of metallic films for vertical-cavity optoelectronic devices. *Appl. Opt.* **1998**, *37*, 5271−5283.
(34) Boles, M. A.; Ling, D.; Hyeon, T.; Talapin, D. V. Erratum: the surface science of nanocrystals. *Nat. Mater.* **2016**, *15*, 364−364.
(35) Mayer, K. M.; Hafner, J. H. Localized surface plasmon resonance sensors. *Chem. Rev.* **2011**, *111*, 3828−3857.
(36) Guo, L.; Jackman, J. A.; Yang, H.-H.; Chen, P.; Cho, N.-J.; Kim, D.-H. Strategies for enhancing the sensitivity of plasmonic nanosensors. *Nano Today* **2015**, *10*, 213−239.
(37) Johnson, P. B.; Christy, R.-W. Optical constants of the noble metals. *Phys. Rev. B* **1972**, *6*, 4370.
(38) Querry, M. R. *Optical constants*. Contractor Report CRDC-CD-85034, **1985**. (Bibcode: https://ui.adsabs.harvard.edu/abs/1985umo..rept···.Q).
(39) Jung, H.; Cha, H.; Lee, D.; Yoon, S. Bridging the nanogap with light: continuous tuning of plasmon coupling between gold nanoparticles. *ACS Nano* **2015**, *9*, 12292−12300.
(40) Nordlander, P.; Oubre, C.; Prodan, E.; Li, K.; Stockman, M. I. Plasmon hybridization in nanoparticle dimers. *Nano Lett.* **2004**, *4*, 899−903.
(41) Persson, B.; Baratoff, A. Theory of photon emission in electron tunneling to metallic particles. *Phys. Rev. Lett.* **1992**, *68*, 3224.
(42) Lambe, J.; McCarthy, S. Light emission from inelastic electron tunneling. *Phys. Rev. Lett.* **1976**, *37*, 923.
(43) Zuloaga, J.; Prodan, E.; Nordlander, P. Quantum description of the plasmon resonances of a nanoparticle dimer. *Nano Lett.* **2009**, *9*, 887−891.
(44) Zhu, W.; Esteban, R.; Borisov, A. G.; Baumberg, J. J.; Nordlander, P.; Lezec, H. J.; Aizourua, J.; Crozier, K. B. Quantum mechanical effects in plasmonic structures with subnanometre gaps. *Nat. Commun.* **2016**, *7*, 1−14.
(45) Ma, Y.; Kalt, R. A.; Stemmer, A. Local strain and tunneling current modulate excitonic luminescence in MoS2 monolayers. *RSC Adv.* **2022**, *12*, 24922−24929.

https://doi.org/10.1021/acsphotonics.4c01408
ACS Photonics XXXX, XXX, XXX−XXX